High-resolution non-line-of-sight imaging employing active focusing

Ruizhi Cao[1], Frederic de Goumoens[1], Baptiste Blochet[1], Jian Xu[1], and Changhuei Yang[1,2]

[1]Department of Electrical Engineering, California Institute of Technology, Pasadena, CA, USA
[2]chyang@caltech.edu

Abstract

Non-line-of-sight (NLOS) imaging is a rapidly developing research direction that has significant applications in autonomous vehicles, remote sensing and other areas. Existing NLOS methods primarily depend on time-gated measurements and sophisticated signal processing to extract information from the scattered light. Here, we introduce a method that directly manipulates the light to counter the wall's scattering. This method, termed Unseen Non-line-of-sight Casted Optical aperture Visibility Enhanced Return (UNCOVER) focusing, operates by actively focusing light onto the hidden target using wavefront shaping. By raster scanning that focus, we can actively image the hidden object. The focus thus formed is near diffraction limited and can be substantially smaller than the object itself, thereby enabling us to perform NLOS imaging with unprecedented resolution. We demonstrate that a resolution of ~ 0.6 mm at a distance of 0.55 m is achievable in UNCOVER, giving us a distance-to-resolution ratio of ~ 970.

1 Introduction

Over the past few decades, significant progress has been made in overcoming scattering in turbid media [1, 2, 3, 4, 5, 6, 7, 8, 9, 10, 11]. Wavefront shaping [1, 2, 3, 4, 5, 6, 7] and multi-photon microscopy [8, 9, 10, 11] are the two main approaches that address scattering. Multi-photon microscopy mitigates scattering by using light of a longer wavelength, as they intrinsically undergo fewer scattering events than light of shorter wavelengths [10, 11]. In contrast, wavefront shaping methods directly counter scattering by actively controlling the wavefront of light [1, 2, 3, 4, 5, 12, 13].

Recently, there has been significant progress in another research area that deals with scattering – non-line-of-sight (NLOS) imaging [14]. A typical NLOS imaging scenario can be described as follows: The target object is hidden from an observer's direct line-of-sight view and only light from the non-line-of-sight path is detected. Typically, the light is passively scattered by the wall and then being detected. The scattering of the wall prevents the observer from collecting a clear image of the object. Nevertheless, it has been shown that it is possible to image the object with novel optical approaches, such as speckle correlations [15, 16], time of flight (ToF) imaging [17, 18, 19], phasor field [20, 21, 22], and other computational imaging methods [23]. These methods do not directly counteract scattering. Instead, they extract useful information from complex signals that usually come with a big background. Existing NLOS methods, which use no prior information of the wall, do not provide diffraction limited resolution. These NLOS imaging methods that are implemented at a practical wall-object distance (> 0.1 m) generally produce modest distance-to-resolution ratios (approximately the inverse of the angular resolution in radian, the distance here is the wall-to-object distance) – ~ 100 is the best number being reported so far [18, 19, 20, 21].

These limitations motivate the use of wavefront shaping. However, the straight translation of wavefront shaping technology for NLOS imaging is infeasible. In wavefront shaping, a guidestar is generally needed [5, 24, 25, 26, 27, 28].

Here, we introduce a new wavefront shaping method, termed Unseen Non-line-of-sight Casted Optical aperture Visibility Enhanced Return (UNCOVER) focusing. UNCOVER uses the hidden object itself as the guidestar and generates a near-diffraction-limited focus that is substantially smaller than the object, which can be raster-scanned to image the object (with its actual 3D coordinates remaining unknown). We note that there are prior wavefront shaping works that can produce a focus that is smaller than the guidestar [26, 27, 28], UNCOVER differs from these methods in that it does not require direct modulations (such as ultrasonic modulation) on the object. Thus, it is well suited for the NLOS settings.

We further note that there are prior wavefront shaping based NLOS imaging works that involve measuring the wall's wavefront scattering characteristics prior to inserting a hidden object [29, 30]. Ref. 29 uses a point source as the initial guidestar, while Ref. 30 uses a camera as a guidestar proxy. Both UNCOVER and Ref. 30 use spatial light modulators to correct the scattered wavefront and use linear phase ramp to raster-scan the generated focus [30, 31, 32]. UNCOVER is different in that it enables NLOS imaging without any prior manipulation of the hidden scene.

UNCOVER achieves a distance-to-resolution ratio of 970 and can image objects with high reflectance differences.

2 Principle

In UNCOVER, we measured the phase variation induced by the wall on the reflected light, and engineer a wavefront that focuses at the target when reflecting off the wall. Unlike general wavefront shaping methods, UNCOVER uses the fact that the wall is a 2D thin scattering object. By imaging the wavefront onto the wall, the angular aperture of the illumination from the wall to the object can be controlled in the wavefront shaping process. Through this process, UNCOVER is able to generate a tight optical focus (smaller than the hidden object) at the object.

An illustration of the UNCOVER system is shown in Fig. 1. The system is optically configured so that the spatial light modulator (SLM), the adjustable input pupil (implemented with a digital micro-mirror device, DMD, in our experiment) and the wall are an image-forming conjugate plane set. The light transmitted through the SLM is imaged onto the wall and its diffuse reflection illuminates the object. The return light from the object scatters off the wall once again. This return light is not wavefront-shaped and is diffusely collected by a detector (see Fig. 1) – we can reasonably assume that the detected signal is proportional to the total light power reflected by the object.

In UNCOVER, our goal is to use the SLM and DMD to project an engineered wavefront that can counter the spatial varying phase shift associated with reflection from the wall towards the object. The reflection off the wall will render a tight and scannable optical focus at the object where the size of the focus is substantially smaller than the object itself. From optical geometry, we expect that the achievable focus spot size is related to the subtended illumination angular aperture at the wall, which depends on the magnification power of the imaging system, the distance between the wall and the hidden object, and the pixel size of the SLM/DMD. As the input pupil and the wall are image-forming conjugate planes, we can control the achievable spot size by controlling the aperture size on the wall. If the object is too large and it is unable to achieve the required de-magnification power in practice, gating methods can be utilized (Supplementary Note Section 2.4). A fully opened pupil (corresponds to full aperture) in combination with the correct pattern displayed on the SLM should render a diffraction-limited focal spot on the object, as shown in

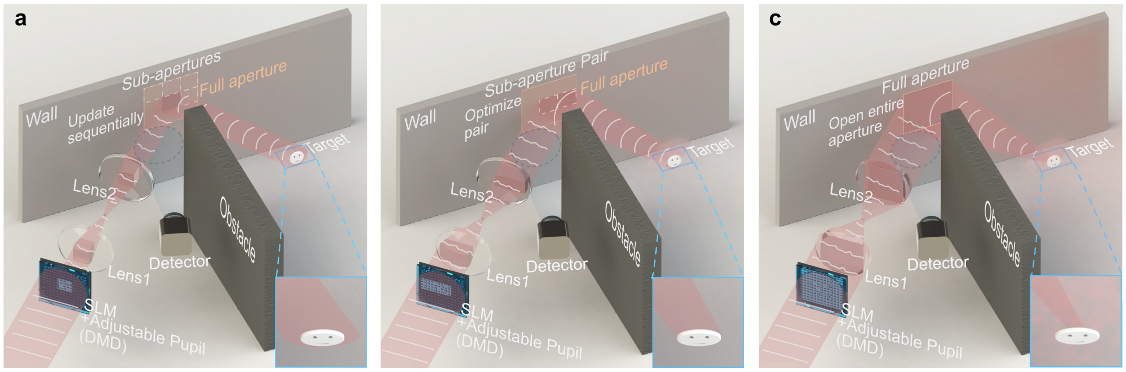

Figure 1: Concept of the system setup. A spatial light modulator (SLM) is imaged onto the wall and modulates the transmitted wavefront. A adjustable pupil (implemented with a digital micromirror device, DMD) is used to control the illuminated area (aperture) on the wall. **a**, UNCOVER firstly optimizes the wavefront transmitted by a small pupil (corresponds to a sub-aperture on the wall) to focus light onto the target. Optimal wavefront is obtained by maximizing the feedback signal. Size of the sub-aperture is chosen to be small enough so that the diffraction-limited focus generated by this sub-aperture is substantially larger than the object itself (nominally by a factor of 2). We repeat the process for a sequence of sub-apertures. The optimized wavefront for each sub-aperture is then treated as a macro-mode. **b**, Next, we select a pair of adjacent sub-apertures and adjust the (relative) phase offset between their macro-modes to maximize reflection from the object. The optimized pair create a diffraction-limited focus that is approximately the size of the object itself. This process is repeated for all sub-aperture pairs and the optimal phase mask is obtained when this process finishes. **c**, By transmitting light through all the sub-apertures simultaneously (i.e. through the full aperture) with the optimized phase mask, a sharp, diffraction-limited focus is generated at the "center" of the object. This final focus is significantly smaller than the object and is raster scanned to obtain an image of the hidden object. The scales and angles shown in the illustration are different from our actual implementation.

Fig. 1c. Mathematically, the relationship between the full aperture size at the wall and the focal spot size (characterized by its full width at half maximum, FWHM) is equal to $\frac{\lambda d}{s}$, where s is the lateral size of the full aperture, λ the wavelength of the light, and d the distance from the wall to the target. By leveraging the wall's optical memory effect [33] and superposing a suitable spatial phase ramp on the SLM phase pattern, we should be able to scan the focal spot across the object and its surrounding (Fig. 2). The determination of the correct SLM phase pattern is the central goal of UNCOVER. This is accomplished in UNCOVER through a 3-step process. In the following discussion, the (sub-) aperture refers to the illuminated area on the wall.

In Step 1, we partition the full aperture into Q sub-apertures. We select the size of the projected sub-apertures on the wall so that two adjacent, optimized sub-apertures would render a diffraction-limited focal spot at the object that is considerably larger than the object's size for the correct SLM phase pattern (the reason will become clear later). That is, one optimized sub-aperture would render a diffraction-limited spot that is substantially larger than the object itself (nominally by a factor of 2 laterally). In this case, it can be proven that the hidden object can be treated as a point (Detailed requirement and its derivation can be found in Supplementary Note Section 2).

In Step 2, we adjust the DMD to project one such sub-apertures. Our goal in this step is to find the correct SLM phase pattern which focuses light onto the object. We further note that the SLM and the DMD are part of the same image-forming conjugate set. To find the correct wavefront solution for one of the sub-apertures, phases of a relatively small number of SLM pixels are modulated such that the feedback signal measured by the detector (Fig. 1) is maximized. The

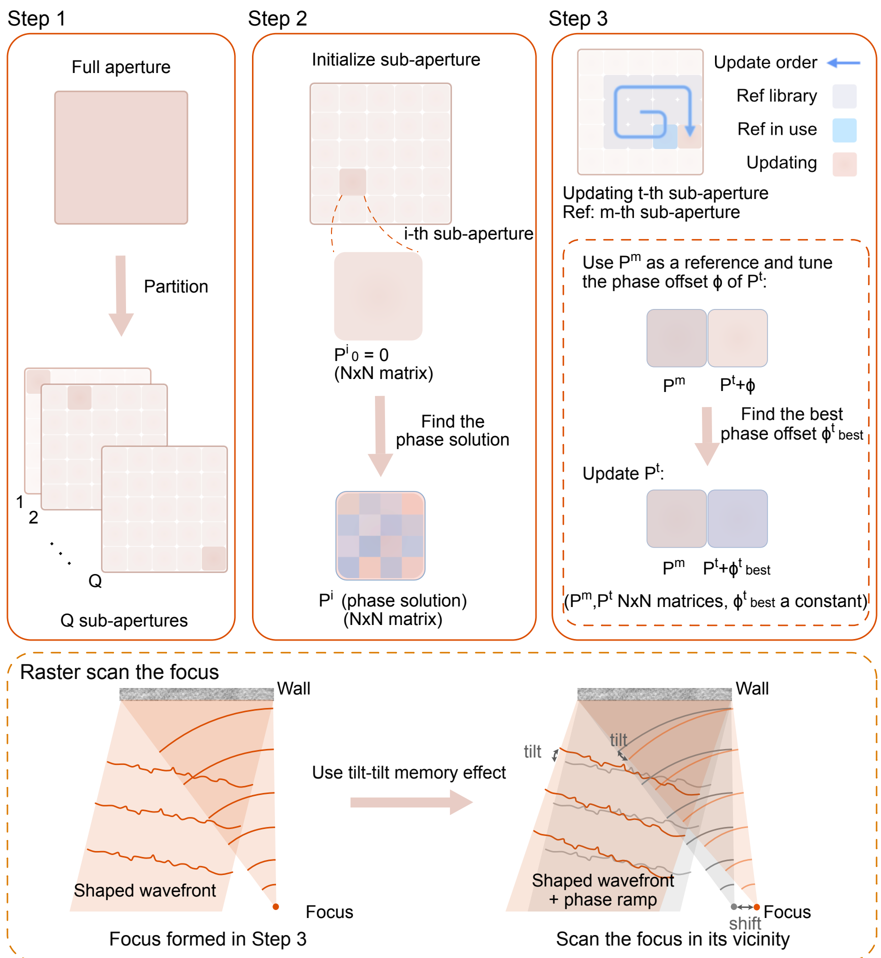

Figure 2: Step by step procedure for UNCOVER. Pupil segmentation is performed in step 1 such that the focus generated by two adjacent sub-apertures is larger than the object. In step 2, phase solutions for each sub-aperture are optimized individually using iterative feedback-based wavefront shaping methods. In step 3, one of the sub-apertures (sub-aperture m in the figure) are used as the reference and a global phase offset is added to the other adjacent sub-aperture (sub-aperture t). By maximizing the feedback signal, the phase solution P^t for sub-aperture t is updated by adding the best phase offset Φ^t_{best}. Here, Q, N, i, m and t are integers. P^k denotes phase mask for the k-th sub-aperture, which is a N-by-N matrix. Once the focus is generated on the target, such focus can be raster scanned, with the help of tilt-tilt memory effect, in the surrounding of the object to generate an image.

determination of the right SLM phase pattern follows a fairly standard wavefront shaping strategy. In our experiments, we used a Hadamard pattern based search process [6, 4, 24, 12, 34], but we can expect most other feedback-based wavefront shaping strategies to work as well. We repeat this procedure for each of the Q sub-apertures. At the end of Step 2, we can treat the determined SLM phase solution for each sub-aperture as a macro-mode. Each macro-mode should focus light at the object with the focal spot size that is diffraction limited (approximately twice the size of the object itself).

In Step 3, we need to determine the correct phase relationship between the sub-aperture macro-modes to synthesize a full aperture, which generates a diffraction-limited focal spot at the object. To accomplish this, we start by opening up 2 adjacent sub-apertures and displaying their corresponding phase patterns on the SLM. One of these patterns will serve as the reference and we will adjust the global phase offset of the other to maximize the return feedback signal from the object. We note here that the optimized pair should now render a diffraction-limited focal spot that is approximately the size of the object itself. More importantly, this focal spot is definitively no smaller than the target so the target can still be treated as a point. Having found the correct global phase relationship for these two sub-apertures, we will then repeat the process with the next adjacent sub-apertures, and so forth. In our experiments, we perform this global phase determination process by selecting sub-apertures in a spiral sequence as shown in step 3 of Fig. 2. This process is akin to the standard feedback-base wavefront shaping procedure, except we are treating each sub-aperture as a macro-mode and simply adjusting each sub-aperture's global phase using pairs consisting of two adjacent sub-apertures, which confine the size of the focus in the optimization. We do not conduct this optimization for sub-apertures that are not adjacent to each other.

At the completion of Step 3, light from all sub-apertures should interfere constructively at the center of mass of the object's reflection function (derivations can be found in Supplementary Note Section 2). By using the pairs in UNCOVER, we can find the relative phase offsets so that light from all sub-apertures will constructively interfere at the center of the target. Applying this optimal phase offset and using the full aperture, the rendered focus should be significantly smaller than the object. This ability to use the object as the guidestar and yet render a smaller-than-object and near-diffraction-limited focus at the object is a key innovation in UNCOVER. The focal spot is then scanned across the object by imposing a spatial phase ramp on the global phase pattern found in Step 2. The extent by which we can shift the focal spot is determined by the optical memory effect range associated with the wall and is related to the wall roughness [33, 32].

3 Result

Our proof-of-concept UNCOVER experiment setup is shown in Fig. 3. A continuous-wave laser diode (DJ532-40, Thorlabs) is used as the light source. The laser beam passes through two mirrors and a half-wave plate (HWP) and is coupled into a polarization maintaining fiber (PM fiber) for spatial filtering. The half-wave plate is used to align the polarization of the laser to the fast axis of the PM fiber and the mirrors are used to couple the light into the fiber. The filtered light exiting the fiber is expanded to fully cover the active area of SLM (Pluto NIR II, phase only SLM, Holoeye). The beamsplitter (BS) and the 4f system (depicted as L3 and L4 in Fig. 3) images the wavefront shaped light reflected by the SLM onto the DMD (DLP lightcrafter 6500 evaluation module, Texas Instrument). The zoom lens (L3; Canon EF-S 18-55 mm) is used to match the different pixel sizes on SLM and DMD. DMD is pixel-to-pixel conjugated to SLM and used to select the sub-aperture to use in the optimization step. A mirror and a second 4f system then project the DMD reflection onto the wall. And the reflection from the wall finally impinges on the object. In our experiment, we use a diffuse reflector (Thorlabs, DG10-1500-P01) as the wall proxy. A photomultiplier tube (PMT, H9306-03, Hamamatsu) and a condenser lens (Thorlabs, ACL50832U-A) are used to collect the light that returns from the object by way of diffuse reflection from the wall. The floor is covered with black papers to minimize the stray light and ensure the bright object is well-defined. Signals from both DMD and PMT are recorded using a data acquisition card (DAQ, PCI-MIO-16XE-10, National Instrument). After the UNCOVER wavefront optimization has been completed, a neutral density filter (ND) is inserted prior to raster scanning to prevent the light from saturating the PMT. The DMD's modulation determines the sub-apertures used in the optimization process. The number of sub-apertures (Q) and number of independent modes (N^2) in each sub-aperture will be specified for each experiment. The optimization process pipeline for UNCOVER can be found in Supplementary Note Section 1.

After we determine the correct wavefront solution for each sub-aperture (Step 2), we would then use sub-aperture pairs to find the phase offset among all the sub-apertures. The pre-defined

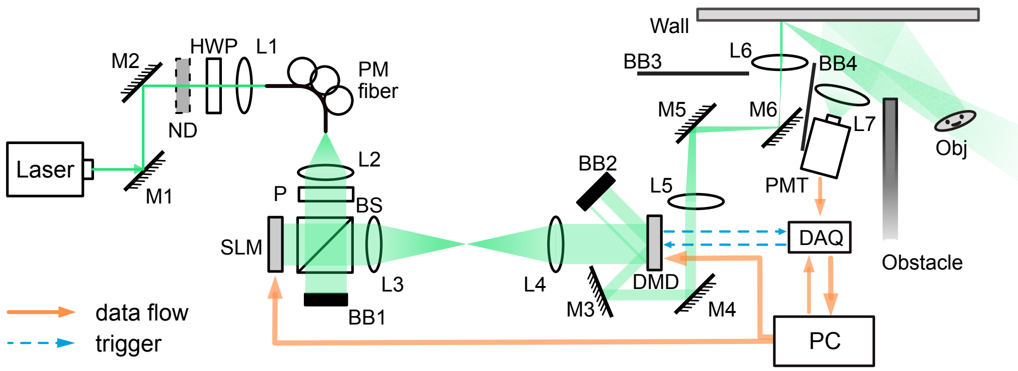

Figure 3: System setup. Light is spatially filtered using the polarization maintaining fiber (PM fiber) and then gets expanded. The spatial light modulator (SLM) and digital micro-mirror device (DMD) are pixel-to-pixel conjugated using the 4f system consisted of L3 and L4. Then DMD is conjugated onto the wall by another 4f system (L5 and L6). DMD's spatial on-off modulation creates different sub-apertures. BB: beam block, BS: beam splitter, DAQ: data acquisition device, HWP: half-wave plate, L: lens, M: Mirrors, ND: neutral density filter, Obj: object, and PMT: photomultiplier tube. In our experiment, SLM/DMD is projected onto a reflective ground glass (wall proxy). Light passes through L6 is normal to the wall surface and the angle between this incident light and the scattered light reaching the target is around 32 degrees in our experiment. The object is also approximately normal to the incident light. BB3 and BB4 are used to minimize the stray light in our system. The floor is covered with black papers to ensure the bright object is well-defined and to minimize the stray light.

sub-aperture pairs are loaded to DMD before the optimization to improve speed. We then update the relative phase between the pair in use. We repeat this process until all the relative phases are optimized. (Fig. S2 in Supplementary Note) A tight focus is then generated when we actuate the DMD for full aperture transmission. We can then impose a linear spatial phase ramp on the SLM wavefront solution to raster scan the focus at the object. The scan range is determined by the tilt-tilt memory effect supported by the wall. In our experiments, our wall proxy has a tilt-tilt memory effect range of 2°, where the angle is measured when the intensity of the focus drops by half while using the largest synthetic aperture.

The first experiment is shown in Fig. 4. An object target was created by placing a patterned black mask (the nominal size of the target was 4 mm) on a diffuse reflector (Thorlabs, DG10-1500-P01). The object was placed 0.3 m away from the wall. The PMT was placed 0.35 m away from the wall. The object and the PMT's direct line of sight was blocked by an obstacle. The mean measurement time for each feedback signal is 40 ms in Step 2. In this experiment, $Q = 64$ sub-apertures and each with $N^2 = 64$ independent modes were used. After performing the UNCOVER optimization process, we were able to render a focus on the object (Fig. 4 a3-c3). We then raster scanned the focus across the object and measured the PMT signal to render a UNCOVER image of the object. For each UNCOVER image pixel, we measured the PMT signal for 100 ms.

In this experiment, the measured focal spot size (FWHM) at the object is 0.55 mm. This measurement was acquired by replacing the object with a camera. The measured spot size is close to the diffraction limited spot size ($\sim$ 0.35 mm in this setting) – indicating that UNCOVER is indeed able to provide close to diffraction limited focusing. Additionally, the distance-to-resolution ratio was determined to be 550. For all three target shapes shown in Fig. 4, the measured focus spot size was relatively unchanged. It is additionally worth noting that the spot size is $\sim$ 7 times smaller than the targets – clearly demonstrating that UNCOVER is capable of generating a focus smaller than the object and is thus able to support imaging. The scanned UNCOVER images are

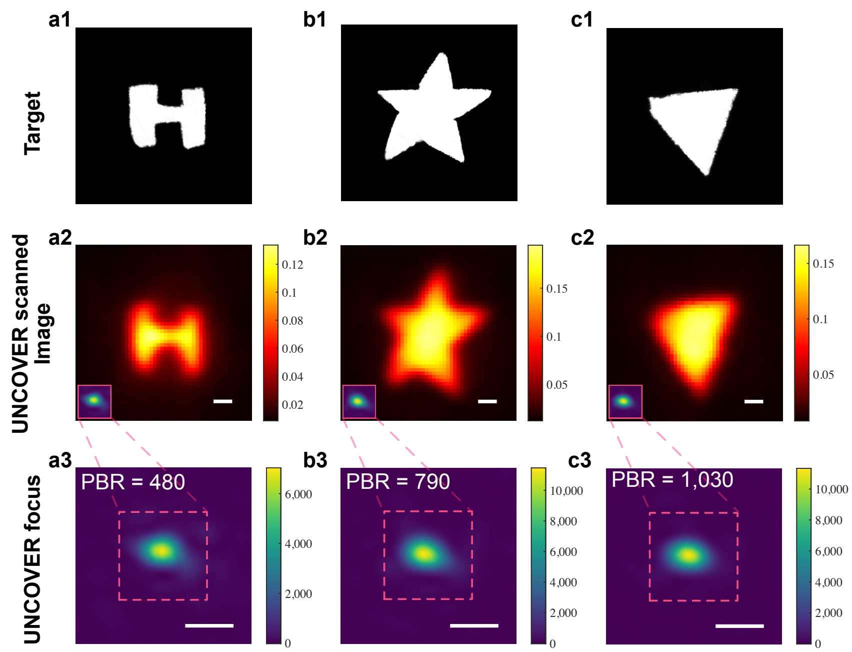

Figure 4: UNCOVER results using different targets. **a1-c1**, the ground truth of the target. **a2-c2**, results of UNCOVER. The inserted figure on the lower left of **a2-c2** is the focus in the dashed square of **a3-c3**, respectively. And it is adapted to have the same scale with respect to the scanned image. **a3-c3**, the image of the optimized foci. The measured peak-to-background ratio (PBR) is shown as well. The result is acquired using $Q = 64$ sub-apertures, with $N^2 = 64$ independent modes in each sub-aperture. A square of 9 by 9 pixels on SLM is treated as one mode. The total illuminated area is a square with side length of approximately 0.35 mm. Scale bars: 1 mm.

shown in Fig. 4, demonstrating good correspondence to the target shapes.

The peak-to-background ratio (PBR) of the focus was also measured for all three shapes. The theoretical PBR should only scales as the number of SLM pixels used by UNCOVER. In this experiment, the theoretical PBR should be equal to 3220. Interestingly, our measured PBR for the three shapes varies significantly, ranging from 480 to 1030. This variation and discrepancy from the theoretical prediction is attributable to the fact that our measurements are noisy. In future experiments, this issue can be mitigated by using a higher power light source and/or by reducing stray light. The degradation of our measured PBR due to noise is consistent with our observation that our lowest measured PBR came from the experiment with the H-shaped target. That target reflected the least light and, as such, gave us the lowest SNR to work with. To study the PBR one can achieve under different initial conditions, we performed additional simulations and the results can also be found in Supplementary Note Section 3.

As UNCOVER generates a scannable optical focus at the object, it is possible for us to raster scan the generated focus beyond the object and image neighboring objects within the range supported by the wall's memory effect. This is potentially an advantage for UNCOVER for imaging dim objects in the presence of bright objects. Bright objects and their associated higher noise can overwhelm the contributions of dimmer objects in standard NLOS method, leading to a diminished imaging dynamic range during image rendering. UNCOVER's ability to focus light on a dim object should allow us to exclude contributions from bright objects when we are attempting to image a dim object.

To study this, we prepared a composite object consisting of a square target placed next to the

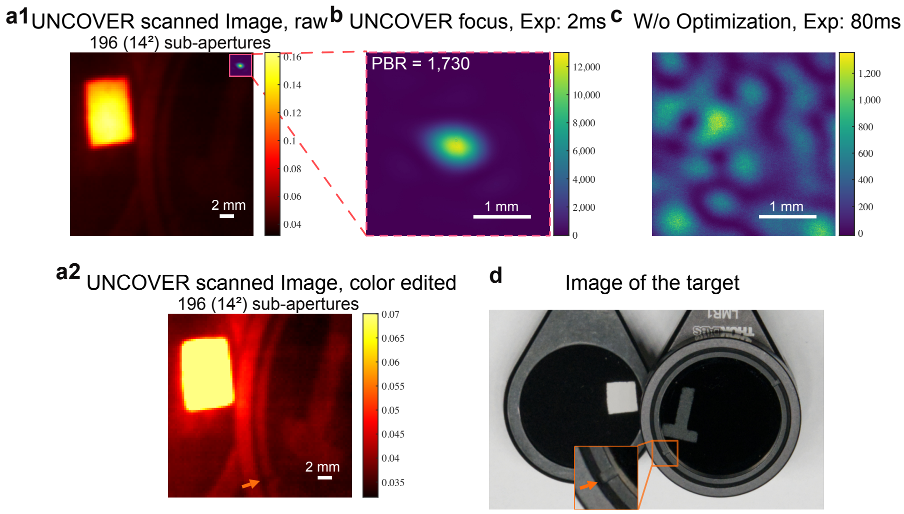

Figure 5: UNCOVER scanning result of two targets whose reflection coefficients differ greatly. **a1**, the raw image from UNCOVER. Inset on the upper right of **a1** is adapted such that the image and the focus are on the same scale. **a2**, result with the maximum signal being capped at 0.07 to make the 'T' shape object more visible. **b**, the focus produced by UNCOVER. **c**, the speckle pattern before optimization. **d**, the target used in this experiment. The brighter square type object is 0.55 m away from the wall. An OD = 0.6 ND filter is placed in front of the 'T' shape object, which reduces its reflection coefficient to 6.3% when comparing with its original reflection coefficient. The arrows in **a2** and **d** show the resolved slot of the retaining ring. In this experiment, a square of side length ≈ 0.61 mm is illuminated when using the full aperture.

'T' target. A ND filter was placed in front of the 'T' target so that the diffuse reflection from it is 16 times weaker than the square target's reflection. In this experiment, the object was placed 0.55 m from the wall. The PMT is 0.5 m away from the wall. Here, we used $Q = 196$ sub-apertures each with $N^2 = 64$ independent modes to achieve a higher lateral resolution and a more uniform background. The mean measurement time for generating one feedback signal in Step 2 is 600 ms. For each UNCOVER image pixel, we measured the PMT signal for 400 ms. From the result (Fig. 5 a1 and a2), the weaker target is clearly resolved in the scanned image. In fact, the return signal from the weaker object is 2.5 times higher than the null background. When both this ratio and the relative reflection difference between the weak and primary objects are taken into consideration, this implies the contrast range of our system is ~ 40. In terms of resolution performance, the measured resolution here is 0.57 mm (FWHM) and the measured distance-to-resolution ratio is 970 in this experiment (the theoretical limit is ~ 1430 for this experiment).

UNCOVER's ability to provide large contrast variation accommodation compares well with the performance of the state-of-the-art ToF based NLOS method, in which the intensity of the reconstruction artifact can be comparable to the primary object [20].

4 Discussion and Conclusion

We demonstrated that UNCOVER can be used to generate a scannable diffraction limited focus that is significantly smaller than the target for NLOS imaging. UNCOVER deviates significantly from standard NLOS method in that it noninvasively forms a small scannable focus at the object.

A direct advantage of such an active focusing based NLOS imaging approach is that it is capable of performing diffraction limited imaging. In our experiment, we demonstrated a prototype system capable of generating a focus spot of size 0.57 mm at a distance of 0.55 m from the wall. This spot size compares favorably with the theoretical limit of 0.37 mm. Additionally, we experimentally demonstrated a distance-to-resolution ratio of 970 in our experiment. This performance specification significantly exceeds the best reported distance-to-resolution ratio of ~ 100 in previous state-of-the-art NLOS experiments using no prior information of the wall [18, 19, 20, 21].

Our experiments also demonstrated that it is possible to redirect the UNCOVER generated focus onto a dimmer object to image the dimmer object. In doing so, we can reduce the return signal from the brighter object and, in turn, allow us to better isolate the signal contribution from the dimmer object. Furthermore, we demonstrated a contrast range of 40 in our experiments, which compares well with standard NLOS methods which suffers from isolating signal contributions from dimmer object in post-processing. Our demonstration experiments were not optimized to maximize the image contrast dynamic range. In future experiments, it would be interesting to explore the bounds of this range, as well as to formalize a mathematical framework to understand its theoretical limit.

We note that our UNCOVER demonstration prototype was not optimized for speed. The process of UNCOVER optimization in our experiments was very much limited by the low laser power and the slow refresh rate of the SLM. Finding the correct wavefront solution to render a UNCOVER focus showed in Fig. 4 a2-c2 required a total time of ~ 40 minutes. Generating the UNCOVER image in Fig. 4 a3-c3 took another 10 minutes. We expect this time can be significantly reduced by switching to high power lasers and faster wavefront shaping methods, such as those based on the use of DMDs, ferroelectric SLM, etc.

At first glance, it may appear that UNCOVER has violated one of the tenets of wavefront shaping – it is not possible to generate a focal spot that is smaller than the homogeneous guidestar/object [31] with linear feedback. UNCOVER overcomes this limitation by novelly exploiting the fact that the wall is a 2D scattering object and that it is possible to control the angular aperture on the wall itself. It is further worth noting that the singular and well-behaved focused spot is generated at the object reflection profile's center-of-mass, even if that location is not reflective at all (see Supplementary Note Section 6).

UNCOVER's field-of-view (or lateral scan range) is limited by the tilt-tilt optical memory effect range of the wall. The wall proxy in our experiments afforded us a fairly large memory effect range (2 degrees). At a wall-to-object distance of 0.55 m, this corresponds to a nominal FOV of 4 cm laterally. We caution that this is a significant underestimation, as the focused peak can persist strongly (PBR $\gg 1$) beyond several multiples of memory range using the model established by Osnabrugge et. al [32]. We additionally note that a rougher wall surface would provide a much narrower memory effect range (for example, 0.33 degrees for a piece of paper) [29, 33] . This topic requires a more complete study as UNCOVER's FOV is a complex function of the memory effect range, initial focus' PBR and hidden targets' reflection profile. We further note that the UNCOVER's FOV can be extended by optimizing for multiple foci at different locations, so that their total field-of-view will provide a much large constitutive coverage. To generate multiple foci, we may need to actively confine the spatial range of the photons that UNCOVER selectively detected. In this context, ToF gating of photons may be quite useful as a selection mechanism. Gating methods are also needed when there are multiple large, bright objects, as discussed in Supplementary Note Section 2.4.

The angular scattering profile of the wall only impacts UNCOVER in its ability to collect photons effectively – a weakly scattering wall will reduce the overall transmission and UNCOVER would have to increase measurement time to compensate. The entire UNCOVER process of generating a focus spot is independent of the wall's scattering profile.

Finally, as with all other active illumination NLOS imaging methods, UNCOVER has a detection signal that drops off as a steep d^4 function (d^2 from illumination multipled by d^2 from light diffused back to the wall), where d is the distance from wall to target. This is a fundamental problem that confounds all active illumination NLOS imaging methods, and that ultimately provides a hard bound on the NLOS imaging range when light budget and imaging time are specified. UNCOVER has the potential to extend this range, in comparison to ToF NLOS methods. This is because ToF methods generally confine the area of detection in order to encode the shape of the target into the time differences of the arriving photons. This confinement restricts the photons that are used in the imaging process. In contrast, UNCOVER can fully utilize almost all the photons (except the one returns back to the full aperture) returning from the object via the wall. This boost in photon utilization rate can in turn be traded off for a longer NLOS imaging range. It is also interesting to note that this ability implies that UNCOVER detection signal is almost independent of the wall-to-detector distance – another signal advantage versus most ToF NLOS methods. We report a brief investigation on this point in Supplementary Note Section 8. The UNCOVER signal dependency is worth a more extended and detailed future study.

In conclusion, we report a novel active focusing based NLOS imaging method that is able to generate a diffraction-limited smaller-than-guidestar focus for raster scanning the hidden object without any prior manipulation of the hidden scene. UNCOVER also broke new wavefront shaping ground by demonstrating that by controlled angular aperture on a scattering surface, it is possible to render a focused spot that is substantially smaller than the homogeneous guidestar itself. As with other active illumination NLOS imaging methods, there are still engineering challenges that need to be addressed for it to become a broadly useful NLOS imaging technique.

References

[1] Vellekoop, I. & Mosk, A. Focusing coherent light through opaque strongly scattering media. *Optics Letters*. **32**, 2309-2311 (2007), https://www.osapublishing.org/ol/abstract.cfm?uri=ol-32-16-2309

[2] Yaqoob, Z., Psaltis, D., Feld, M. & Yang, C. Optical phase conjugation for turbidity suppression in biological samples. *Nature Photonics*. **2**, 110-115 (2008), https://www.nature.com/articles/nphoton.2007.297

[3] Popoff, S., Lerosey, G., Fink, M., Boccara, A. & Gigan, S. Image transmission through an opaque material. *Nature Communications*. **1** pp. 81 (2010), https://www.nature.com/articles/ncomms1078

[4] Vellekoop, I. Feedback-based wavefront shaping. *Optics Express*. **23**, 12189-12206 (2015), https://www.osapublishing.org/oe/abstract.cfm?uri=oe-23-9-12189

[5] Xu, X., Liu, H. & Wang, L. Time-reversed ultrasonically encoded optical focusing into scattering media. *Nature Photonics*. **5**, 154-157 (2011), https://www.nature.com/articles/nphoton.2010.306

[6] Conkey, D., Caravaca-Aguirre, A. & Piestun, R. High-speed scattering medium characterization with application to focusing light through turbid media. *Optics Express*. **20**, 1733-1740 (2012), https://www.osapublishing.org/oe/abstract.cfm?uri=oe-20-2-1733

[7] Mosk, A., Lagendijk, A., Lerosey, G. & Fink, M. Controlling waves in space and time for imaging and focusing in complex media. *Nature Photonics*. **6**, 283-292 (2012), https://www.nature.com/articles/nphoton.2012.88

[8] Denk, W., Strickler, J. & Webb, W. Two-photon laser scanning fluorescence microscopy. *Science*. **248**, 73-76 (1990), https://science.sciencemag.org/content/248/4951/73

[9] Xu, C., Zipfel, W., Shear, J., Williams, R. & Webb, W. Multiphoton fluorescence excitation: new spectral windows for biological nonlinear microscopy. *Proceedings Of The National Academy Of Sciences*. **93**, 10763-10768 (1996), https://www.pnas.org/content/93/20/10763

[10] Helmchen, F. & Denk, W. Deep tissue two-photon microscopy. *Nature Methods*. **2**, 932-940 (2005), https://www.nature.com/articles/nmeth818

[11] Horton, N., Wang, K., Kobat, D., Clark, C., Wise, F., Schaffer, C. & Xu, C. In vivo three-photon microscopy of subcortical structures within an intact mouse brain. *Nature Photonics*. **7**, 205-209 (2013), https://www.nature.com/articles/nphoton.2012.336

[12] Popoff, S., Lerosey, G., Fink, M., Boccara, A. & Gigan, S. Controlling light through optical disordered media: transmission matrix approach. *New Journal Of Physics*. **13**, 123021 (2011), https://doi.org/10.1088/1367-2630/13/12/123021

[13] Mounaix, M., Andreoli, D., Defienne, H., Volpe, G., Katz, O., Grésillon, S. & Gigan, S. Spatiotemporal Coherent Control of Light through a Multiple Scattering Medium with the Multispectral Transmission Matrix. *Physical Review Letters*. **116**, 253901 (2016), https://link.aps.org/doi/10.1103/PhysRevLett.116.253901

[14] Faccio, D., Velten, A. & Wetzstein, G. Non-line-of-sight imaging. *Nature Reviews Physics*. **2**, 318-327 (2020), https://www.nature.com/articles/s42254-020-0174-8

[15] Bertolotti, J., Putten, E., Blum, C., Lagendijk, A., Vos, W. & Mosk, A. Non-invasive imaging through opaque scattering layers. *Nature*. **491**, 232-234 (2012), https://www.nature.com/articles/nature11578

[16] Katz, O., Heidmann, P., Fink, M. & Gigan, S. Non-invasive single-shot imaging through scattering layers and around corners via speckle correlations. *Nature Photonics*. **8**, 784-790 (2014), https://www.nature.com/articles/nphoton.2014.189

[17] Velten, A., Willwacher, T., Gupta, O., Veeraraghavan, A., Bawendi, M. & Raskar, R. Recovering three-dimensional shape around a corner using ultrafast time-of-flight imaging. *Nature Communications*. **3** pp. 745 (2012), https://www.nature.com/articles/ncomms1747

[18] O'Toole, M., Lindell, D. & Wetzstein, G. Confocal non-line-of-sight imaging based on the light-cone transform. *Nature*. **555**, 338-341 (2018), https://www.nature.com/articles/nature25489

[19] Xin, S., Nousias, S., Kutulakos, K., Sankaranarayanan, A., Narasimhan, S. & Gkioulekas, I. A Theory of Fermat Paths for Non-Line-Of-Sight Shape Reconstruction. *2019 IEEE/CVF Conference On Computer Vision And Pattern Recognition (CVPR)*. pp. 6793-6802 (2019)

[20] Liu, X., Guillén, I., La Manna, M., Nam, J., Reza, S., Huu Le, T., Jarabo, A., Gutierrez, D. & Velten, A. Non-line-of-sight imaging using phasor-field virtual wave optics. *Nature*. **572**, 620-623 (2019), https://www.nature.com/articles/s41586-019-1461-3

[21] Reza, S., Manna, M., Bauer, S., Velten, A. & Velten, A. Phasor field waves: A Huygens-like light transport model for non-line-of-sight imaging applications. *Optics Express*. **27**, 29380-29400 (2019), https://www.osapublishing.org/oe/abstract.cfm?uri=oe-27-20-29380

[22] Gupta, M., Nayar, S., Hullin, M. & Martin, J. Phasor Imaging: A Generalization of Correlation-Based Time-of-Flight Imaging. *ACM Transactions On Graphics*. **34**, 156:1-156:18 (2015), https://doi.org/10.1145/2735702

[23] Saunders, C., Murray-Bruce, J. & Goyal, V. Computational periscopy with an ordinary digital camera. *Nature*. **565**, 472 (2019), https://www.nature.com/articles/s41586-018-0868-6

[24] Horstmeyer, R., Ruan, H. & Yang, C. Guidestar-assisted wavefront-shaping methods for focusing light into biological tissue. *Nature Photonics*. **9**, 563-571 (2015), https://www.nature.com/articles/nphoton.2015.140

[25] Ruan, H., Jang, M., Judkewitz, B. & Yang, C. Iterative Time-Reversed Ultrasonically Encoded Light Focusing in Backscattering Mode. *Scientific Reports*. **4**, 1-7 (2014), https://www.nature.com/articles/srep07156

[26] Katz, O., Ramaz, F., Gigan, S. & Fink, M. Controlling light in complex media beyond the acoustic diffraction-limit using the acousto-optic transmission matrix. *Nature Communications*. **10**, 1-10 (2019), https://www.nature.com/articles/s41467-019-08583-6

[27] Judkewitz, B., Wang, Y., Horstmeyer, R., Mathy, A. & Yang, C. Speckle-scale focusing in the diffusive regime with time reversal of variance-encoded light (TROVE). *Nature Photonics*. **7**, 300-305 (2013), https://www.nature.com/articles/nphoton.2013.31

[28] Conkey, D., Caravaca-Aguirre, A., Dove, J., Ju, H., Murray, T. & Piestun, R. Super-resolution photoacoustic imaging through a scattering wall. *Nature Communications*. **6**, 7902 (2015), https://doi.org/10.1038/ncomms8902

[29] Katz, O., Small, E. & Silberberg, Y. Looking around corners and through thin turbid layers in real time with scattered incoherent light. *Nature Photonics*. **6**, 549-553 (2012), http://www.nature.com/articles/nphoton.2012.150

[30] Starshynov, I., Ghafur, O., Fitches, J. & Faccio, D. Coherent Control of Light for Non-Line-of-Sight Imaging. *Physical Review Applied*. **12**, 064045 (2019), https://link.aps.org/doi/10.1103/PhysRevApplied.12.064045

[31] Katz, O., Small, E., Guan, Y. & Silberberg, Y. Noninvasive nonlinear focusing and imaging through strongly scattering turbid layers. *Optica*. **1**, 170-174 (2014), https://www.osapublishing.org/optica/abstract.cfm?uri=optica-1-3-170

[32] Osnabrugge, G., Horstmeyer, R., Papadopoulos, I., Judkewitz, B. & Vellekoop, I. Generalized optical memory effect. *Optica*. **4**, 886-892 (2017), https://www.osapublishing.org/optica/abstract.cfm?uri=optica-4-8-886

[33] Freund, I., Rosenbluh, M. & Feng, S. Memory Effects in Propagation of Optical Waves through Disordered Media. *Physical Review Letters*. **61**, 2328-2331 (1988), https://link.aps.org/doi/10.1103/PhysRevLett.61.2328

[34] Jang, J., Lim, J., Yu, H., Choi, H., Ha, J., Park, J., Oh, W., Jang, W., Lee, S. & Park, Y. Complex wavefront shaping for optimal depth-selective focusing in optical coherence tomography. *Optics Express*. **21**, 2890-2902 (2013), https://www.osapublishing.org/oe/abstract.cfm?uri=oe-21-3-2890

Acknowledgement

This research is supported by Caltech Sensing to Intelligence (S2I) (Award Number: 13520296).

Data availability

The data that support the plots within this paper and other findings of this study are available from the corresponding authors upon reasonable request.

Code availability

The code that supports the plots within this paper and other findings of this study is available from the corresponding authors upon reasonable request.

Contributions

C.Y. conceived the idea. R.C., B.B. and J.X developed the idea. R.C. designed and developed the experimental protocol and set-up. R.C. conducted the theoretical analysis, conducted the experiments and wrote the simulation and experiment code. F.G. helped with the simulation code. All authors contributed to the preparation of the manuscript.

Competing interests

The authors declare the following competing interests:

In October 2020, California Institute of Technology filed a patent for UNCOVER (U.S. Application No 63/090,429), which covered the concept and implementation of the UNCOVER system described here.